Bayesian time-lapse difference inversion based on the exact Zoeppritz equations with blockiness constraint

Zhou, Lin; Liao, Jianping; Li, Jingye; Chen, Xiaohong; Yang, Tianchun; Hursthouse, Andrew

Published in:
Journal of Environmental & Engineering Geophysics

DOI:
10.2113/JEEG19-045

Published: 27/05/2020

Document Version
Peer reviewed version

Bayesian Time-lapse Difference Inversion Based on the exact Zoeppritz Equations with Blockiness Constraint

Lin Zhou [1], Jianping Liao [1]*, Jingye Li [2, 3], Xiaohong Chen [2, 3], Tianchun Yang [1], Andrew Hursthouse[1, 4]

[1]Hunan Provincial Key Laboratory of Shale Gas Resource Utilization, Hunan University of Science and Technology, Xiangtan 411201, Hunan, China

[2]State Key Laboratory of Petroleum Resources and Prospecting, China University of Petroleum, Changping 102249, Beijing, China

[3]National Engineering Laboratory for Offshore Oil Exploration, China University of Petroleum, Changping 102249, Beijing, China

[4]School of Computing, Engineering & Physical Sciences, University of the West of Scotland, Paisley PA1 2BE, UK

ABSTRACT

Accurately inverting changes in the elastic parameters of a reservoir that are caused by oil and gas exploitation is of great importance in accurately describing reservoir dynamics and enhancing recovery. Previously numerous time-lapse seismic inversion methods based on the approximate formulas of exact Zoeppritz equations or wave equations have been used to estimate these changes. However the low accuracy of calculations using approximate formulas and the significant calculation effort for the wave equations seriously limits the application of these methods. However, these limitations can be overcome by using exact Zoeppritz equations. Therefore, we study the time-lapse seismic difference inversion method using the exact Zoeppritz equations. Firstly, the forward equation of time-lapse seismic difference data is derived based on the exact Zoeppritz equations. Secondly, the objective function based on Bayesian inversion theory is constructed using this equation, with the changes in elastic parameters assumed to obey a Gaussian distribution. In order to capture the sharp time-lapse changes of elastic parameters and further enhance the resolution of the inversion results, the blockiness constraint, which follows the differentiable Laplace distribution, is added to the prior Gaussian background model. All examples of its application show that the proposed method can obtain stable and reasonable P- and S-wave velocities and density changes from the difference data . The accuracy of estimation is higher than for existing methods, which verifies the effectiveness and feasibility of the new method. It can provide high-quality seismic inversion results for dynamic detailed reservoir description and well location during development.

KEYWORDS: Exact Zoeppritz equations; Time-lapse seismic; Bayesian inversion; Blockiness constraint; Differentiable Laplace distribution

Introduction

Seismic inversion technology can be used to quantify the changes of seismic response caused by oil and gas exploitation, and derive the changes in the elastic parameters of the reservoir. This information can then be combined with the rock physics relationship to predict the changes of hydrocarbon saturation, stress and other physical parameters, and also provide important seismic information for the prediction of residual oil and gas distribution in the middle and late stages of development along with a detailed reservoir description (Landr 2001, Tura and Lumley 1999, Li et al 2005, Grana and Mukerji 2015, Liu et al 2016, Liu et al 2018). Therefore, this technology is widely implemented in reservoir characterization, monitoring and management.

A large number of studies of time-lapse seismic inversion methods have been undertaken. Based on

post-stack seismic data, Gluck et al (2000) studied the inversion of time-lapse seismic wave impedance. Li et al (2011) and Tang et al (2018) studied and tested elastic impedance difference inversion for time-lapse seismic data. Pre-stack seismic data retains more information of subsurface geology than post-stack data. Pre-stack Inversion can obtain more abundant elastic parameter information. Therefore, a large number of studies have been carried out on pre-stack time-lapse seismic inversion. Abubakar et al (2001) studied a nonlinear time-lapse seismic inversion algorithm based on acoustic wave equation. Chen et al (2010) studied time-lapse seismic inversion based on two-dimensional (2D) acoustic equation by using multi-scale total variation method that could improve the accuracy and computational efficiency of the algorithm. Raknes and Arntsen (2015), Hicks et al (2016), Kamei et al (2017), Kamei and Lumley (2017) studied the time-lapse seismic full-waveform inversion methods from different perspectives, and achieved good results. The time-lapse seismic inversion algorithms based on wave equations are difficult to apply to the inversion field data from large three-dimensional (3D) working areas due to high processing demands of the calculations. For this reason research on pre-stack AVO/AVA inversion methods has become popular and have been widely used in field production.

The pre-stack time-lapse seismic AVO/AVA inversion methods include three strategies: independent, joint and difference inversion. Independent inversion uses the existing pre-stack AVO/AVA inversion method to invert the baseline and monitor survey data respectively, subtracts these inversion results, and obtains the changes in elastic parameters of the reservoir (Ayeni et al 2009). Joint inversion means the base and monitor seismic data are used to construct the inversion objective function, and the elastic parameters are obtained corresponding to the baseline survey data and changes in the elastic parameter caused by injection and production (Kato et al. 2010). Difference inversion means that in order to obtain difference data, it is necessary to subtract well matched baseline survey data from monitor survey data, then use these data as input, construct an objective function and solve it, and finally obtain the changes in elastic parameters. Buland and Ouair (2006) and Wang and Wang (2012) realized time-lapse seismic difference inversion based on Bayesian theory. Zhi et al (2016) utilized Gardner's formula to achieve time-lapse seismic AVO difference inversion. In addition to directly invert the changes in elastic parameters, the estimation of reservoir physical parameters changes by combining with the petrophysical model has been studied. Li et al. (2005) proposed a new time-lapse seismic AVO inversion calculation method to effectively separate the oil saturation and effective pressure changes of the reservoir and realized the quantitative interpretation of the reservoir. Grana and Mukerji (2015) studied the Bayesian inversion of time-lapse seismic data for the

estimation of static reservoir properties and dynamic property changes by combining petrophysical relationships. These AVO/AVA time-lapse seismic inversion methods mentioned above are based on the approximate formulae of exact Zoeppritz equations. The low calculation accuracy and poor applicability of the approximate formulae greatly prevent the inversion accuracy of conventional time-lapse seismic inversion methods, making these methods hard to meet the increasingly high accuracy requirements of seismic inversion results in detailed description of reservoir dynamics. The exact equations can solve the problems due to use of the approximate formulas highlighted above. Therefore, we describe out time-lapse AVO seismic inversion based on the Zoeppritz equations. Zhang et al (2013), Lu et al (2015), Zhi et al (2016) and Zhou et al (2016, 2017) proposed the pre-stack inversion method based on the exact Zoeppritz equations from different perspectives. Theoretically, using these methods to carry out the independent time-lapse seismic inversion can not only obtain the changes in elastic parameters, but also overcome the problem of the approximate formulae. However, the coupling of the baseline and monitor survey data is not widely utilized in independent inversion, so this inversion strategy is not the optimal choice. In this regard, Zhi and Gu (2018) utilized the generalized linear inversion method to realize the time-lapse seismic joint inversion based on the exact Zoeppritz equations.

Sarkar et al (2003) pointed out that it is necessary to perform some coupling between the time-lapse seismic data inversion in different years, otherwise it will disrupt the final model, which leads to incorrect inversion results. Difference inversion can provide the necessary coupling conditions. If the repeatability between the base and monitor seismic data is appropriate, the difference in time-lapse seismic inversion is usually the most suitable inversion strategy. Therefore, we study the difference inversion based on the exact Zoeppritz equations.

When using Bayesian theory to construct the inversion objective function, the accuracy and resolution of the inversion results can be further improved by introducing a more reasonable priori model. Eidsvik and Theune (2009) studied blocky inversion method for time-lapse seismic AVO data by introducing a blockiness constrained prior model, and the actual data processing results demonstrated that this method could better reflect the changes of time-lapse elastic parameters. Theune et al (2010) pointed out that the vertical blockiness constraint, obeying the differentiable Laplace distribution, could more reliably capture sharp time-lapse changes in elastic parameters through comparative analysis of different blocky inversion prior models. In addition, the presence of well-matched multi-wave data means that joint inversion can further improve the stability, accuracy and resolution of the inversion results. Stewart (1990) first proposed the

framework of a joint PP-PS wave inversion method. Lu et al (2015) and Zhou et al (2016, 2017) both achieved better results using a Zoeppritz equations based on a joint PP-PS waves inversion method.

Therefore, on the basis of previous studies, we present a new Bayesian time-lapse seismic AVA difference inversion method based on the exact Zoeppritz equations. It is successfully extended to the case of multi-wave inversion. This method derives the forward equation of time-lapse seismic difference data using the exact Zoeppritz equations, and introduces the blocky inversion prior model that follows differentiable Laplace distribution. Finally, high-resolution seismic inversion results are obtained, which provides important information for favorable well placement and risk assessment of injector-production in the middle and later stages of reservoir development.

Methodology

Deriving the Forward Equation

For well-matched time-lapse seismic data, changes in seismic response are usually confined to specific formations, while in non-oil reservoirs, the baseline and monitor survey data should be the same. The difference data is generated by subtracting the monitor survey data from baseline survey data, which can make the two seismic data sets collected at different times derive necessary coupling. The difference data can then be directly inverted to obtain the changes in the elastic parameters of the reservoir caused by exploitation.

The forward equations of baseline and monitor survey data are as follows:

$$\mathbf{d}_1 = \mathbf{G}\left(\mathbf{m}_1\right) + \mathbf{n}_1 \tag{1}$$

$$\mathbf{d}_2 = \mathbf{G}\left(\mathbf{m}_2\right) + \mathbf{n}_2 \tag{2}$$

where, $\mathbf{G}$ is the forward operator of Zoeppritz equations, $\mathbf{d}_1$ is baseline survey data, $\mathbf{d}_2$ is monitor survey data, $\mathbf{m}_1$ is the elastic parameters corresponding to the baseline survey data, $\mathbf{m}_2$ is the elastic parameters corresponding to the monitor survey data, $\mathbf{n}_1$ and $\mathbf{n}_2$ are the noise data for two data sets respectively.

The Taylor series expansion of equation (2) is carried out with the elastic parameters $\mathbf{m}_1$:

$$\mathbf{d}_2 = \mathbf{G}\left(\mathbf{m}_2\right) + \mathbf{n}_2 = \mathbf{G}\left(\mathbf{m}_1\right) + \frac{\partial \mathbf{G}\left(\mathbf{m}_1\right)}{\partial \mathbf{m}} \Delta\mathbf{m} + \mathbf{n}_0 + \mathbf{n}_2 \tag{3}$$

Subtracting equation (1) from equation (3), we have:

$$\Delta\mathbf{d} = \mathbf{d_2} - \mathbf{d_1} = \frac{\partial \mathbf{G}(\mathbf{m}_1)}{\partial \mathbf{m}} \Delta\mathbf{m} + \mathbf{n}_0 + \mathbf{n}_2 - \mathbf{n}_1 \tag{4}$$

Assuming that $\mathbf{L} = \frac{\partial \mathbf{G}(\mathbf{m}_1)}{\partial \mathbf{m}}$, $\mathbf{e} = \mathbf{n}_0 + \mathbf{n}_2 - \mathbf{n}_1$, the following expression is acquired:

$$\Delta\mathbf{d} = \mathbf{L}\Delta\mathbf{m} + \mathbf{e} \tag{5}$$

where, $\Delta\mathbf{d}$ is difference seismic data, $\Delta\mathbf{m}$ is the elastic parameter changes, $\mathbf{L} = \frac{\partial \mathbf{G}(\mathbf{m}_1)}{\partial \mathbf{m}}$ is the first partial derivative of the forward operator matrix based on the exact Zoeppritz equations with respect to three elastic parameters, including P- and S-wave velocities and density (see Appendix A for the derivation), $\mathbf{n}_0$ is the higher order term of the Taylor series expansion, $\mathbf{e}$ is the error term directly related to the difference data, and can also be considered as noise.

Bayesian Time-Lapse Seismic AVA Inversion

Assuming that the error term $\mathbf{e}$ in equation (5) follows the zero-mean Gaussian distribution, the likelihood function can be expressed as:

$$P(\Delta\mathbf{d} \mid \Delta\mathbf{m}) = \left((2\pi)^{N_d} |\mathbf{C}_D|\right)^{-1/2} \exp\left(-\frac{1}{2}(\Delta\mathbf{d} - \mathbf{L}\Delta\mathbf{m})^T \mathbf{C}_D^{-1} (\Delta\mathbf{d} - \mathbf{L}\Delta\mathbf{m})\right) \tag{6}$$

where, $\mathbf{C}_D$ is the covariance matrix of noise, N_d is the length of the observed data. The negative logarithm of the above expression can be expressed as:

$$F(\Delta\mathbf{d} \mid \Delta\mathbf{m}) = \frac{1}{2}(\Delta\mathbf{d} - \mathbf{L}\Delta\mathbf{m})^T \mathbf{C_D^{-1}} (\Delta\mathbf{d} - \mathbf{L}\Delta\mathbf{m}) + const \tag{7}$$

By statistical analysis of the sample point values of logging data, Todoeschuck et al (1990) pointed out that the logging data of the whole logging curve did not conform to the normal distribution, but it follows a normal distribution if only a small part of it was taken for research. Time-lapse seismic inversion usually only inverts the changes of the elastic parameters of the target interval, so it can be considered that the changes of the elastic parameters of this small segment follow a normal distribution. Buland et al (2006) assumed that the changes of the elastic parameters obey a normal distribution, and studied the time-lapse seismic difference inversion method based on Bayesian theory, with good results. Since the difference data has a block phenomenon, blockiness constraint terms are considered to be added to the prior model. According to the research of Theune et al (2010), it is assumed that vertical blockiness constraint term follows the differentiable Laplace distribution. To sum up, the prior model consists of two parts: (1) a

Gaussian distribution term containing the priori low frequency trend and internal covariance among three elastic parameters; (2) a blockiness constraint term with long tail distribution characteristics.

First, assuming that the priori model obeys the Gaussian distribution:

$$P_1\left(\Delta\mathbf{m}\right)=\frac{1}{(2\pi)^{(N/2)}\left|\mathbf{C}_{\Delta\mathbf{m}}\right|^{1/2}}\exp\left(-\frac{1}{2}\left(\Delta\mathbf{m}-\boldsymbol{\mu}\right)^T\mathbf{C}_{\Delta\mathbf{m}}^{-1}\left(\Delta\mathbf{m}-\boldsymbol{\mu}\right)\right) \tag{8}$$

Taking the negative log of equation (8), we can obtain:

$$F_1\left(\Delta\mathbf{m}\right)=\frac{1}{2}\left(\Delta\mathbf{m}-\boldsymbol{\mu}\right)^T\mathbf{C}_{\Delta\mathbf{m}}^{-1}\left(\Delta\mathbf{m}-\boldsymbol{\mu}\right)+const \tag{9}$$

where, $C_{\Delta\mathbf{m}}$ is a covariance matrix that contains the statistical correlation of the three elastic parameters changes, N is the size of model parameters, and $\boldsymbol{\mu}$ is the mean vector of model parameters. Then, in order to obtain sharp parameters changes, the vertical blockiness constraint which follows the differentiable Laplace distribution is added into the prior model, and the negative logarithm of the prior model is defined as follows:

$$F\left(\Delta\mathbf{m}\right)=const+F_1\left(\Delta\mathbf{m}\right)+F_2\left(\Delta\mathbf{m}\right) \tag{10}$$

where $F_2\left(\Delta\mathbf{m}\right)$ represents the blockiness constraint, and its expression is:

$$F_2\left(\Delta\mathbf{m}\right)=const+\sum_{l=1}^{3}\left(\sqrt{1+\frac{\left[\mathbf{D}\left(\Delta\mathbf{m}-\boldsymbol{\mu}\right)\right]_l^T\left[\mathbf{D}\left(\Delta\mathbf{m}-\boldsymbol{\mu}\right)\right]_l}{k_l^2}}-1\right) \tag{11}$$

where, $\mathbf{D}$ is a first-order differential matrix and the $k_l, l=1,2,3$ parameters, are scaling parameters that can be different for each of model parameters. Generally, these scaling parameters can be obtained from logging data by utilizing a maximum likelihood estimator (MLE) (Theune et al 2010)

By substituting equations (7) and (10) into Bayesian theory and canceling out constant terms, the objective function can be obtained as follows:

$$\begin{aligned}J_1\left(\Delta\mathbf{m}\right)=&\frac{1}{2}\left(\Delta\mathbf{d}-\mathbf{L}\Delta\mathbf{m}\right)^T\mathbf{C}_{\mathbf{D}}^{-1}\left(\Delta\mathbf{d}-\mathbf{L}\Delta\mathbf{m}\right)+\frac{1}{2}\left(\Delta\mathbf{m}-\boldsymbol{\mu}\right)^T\mathbf{C}_{\Delta\mathbf{m}}^{-1}\left(\Delta\mathbf{m}-\boldsymbol{\mu}\right)\\&+\sum_{l=1}^{3}\left(\sqrt{1+\frac{\left[\mathbf{D}\left(\Delta\mathbf{m}-\boldsymbol{\mu}\right)\right]_l^T\left[\mathbf{D}\left(\Delta\mathbf{m}-\boldsymbol{\mu}\right)\right]_l}{k_l^2}}-1\right)\end{aligned} \tag{12}$$

Generally, the noise terms of the observed seismic data are assumed to be uncorrelated, so that the matrix $\mathbf{C}_D$ can be reduced to a diagonal matrix. Then, the matrix $\mathbf{C}_D$ can be expressed as, $\mathbf{C}_D=\sigma_n^{\,2}\mathbf{I}$,

where $\sigma_n^{\,2}$ is the noise variance, and $\mathbf{I}$ is an $N_d \times N_d$ identity matrix. For multi-wave seismic data, assuming that the noise variances of the P- and S-wave data are $\sigma_{PP}^{\,2}$ and $\sigma_{PS}^{\,2}$, respectively, then equation (12) can be rewritten as follows:

$$\begin{aligned} J\left(\Delta\mathbf{m}\right) = & \frac{1}{2}\left(\Delta\mathbf{d}_{PP} - \mathbf{L}_{PP}\Delta\mathbf{m}\right)^T \left(\Delta\mathbf{d}_{PP} - \mathbf{L}_{PP}\Delta\mathbf{m}\right) \\ & + \frac{\alpha}{2}\left(\Delta\mathbf{d}_{PS} - \mathbf{L}_{PS}\Delta\mathbf{m}\right)^T \left(\Delta\mathbf{d}_{PS} - \mathbf{L}_{PS}\Delta\mathbf{m}\right) \\ & + \frac{\beta}{2}\left(\Delta\mathbf{m} - \boldsymbol{\mu}\right)^T \mathbf{C}_{\Delta\mathbf{m}}^{-1}\left(\Delta\mathbf{m} - \boldsymbol{\mu}\right) + \beta\sum_{l=1}^{3}\left(\sqrt{1 + \frac{\left[\mathbf{D}\left(\Delta\mathbf{m} - \boldsymbol{\mu}\right)\right]_l^T \left[\mathbf{D}\left(\Delta\mathbf{m} - \boldsymbol{\mu}\right)\right]_l}{k_l^2}} - 1\right) \end{aligned} \tag{13}$$

where $\alpha = \sigma_{PP}^{\,2} / \sigma_{PS}^{\,2}$ controls the weight of the shear wave data, and $\beta = \sigma_{PP}^{\,2}$ controls the weight of the prior information.

By differentiating the above equation with respect to $\Delta\mathbf{m}$ and equating the result to zero, we can obtain:

$$\begin{aligned} & \left(\mathbf{L}_{PP}^T\mathbf{L}_{PP} + \alpha\mathbf{L}_{PS}^T\mathbf{L}_{PS} + \beta\left(\mathbf{C}_{\Delta\mathbf{m}}^{-1} + \mathbf{D}^T\mathbf{A}\mathbf{D}\right)\right)\Delta\mathbf{m} \\ & = \mathbf{L}_{PP}^T\Delta\mathbf{d}_{PP} + \alpha\mathbf{L}_{PS}^T\Delta\mathbf{d}_{PS} + \beta\left(\mathbf{C}_{\Delta\mathbf{m}}^{-1} + \mathbf{D}^T\mathbf{A}\mathbf{D}\right)\boldsymbol{\mu} \end{aligned} \tag{14}$$

giving

$$\begin{aligned} \Delta\mathbf{m} = & \left(\mathbf{L}_{PP}^T\mathbf{L}_{PP} + \alpha\mathbf{L}_{PS}^T\mathbf{L}_{PS} + \beta\left(\mathbf{C}_{\Delta\mathbf{m}}^{-1} + \mathbf{D}^T\mathbf{A}\mathbf{D}\right)\right)^{-1} \\ & * \left(\mathbf{L}_{PP}^T\Delta\mathbf{d}_{PP} + \alpha\mathbf{L}_{PS}^T\Delta\mathbf{d}_{PS} + \beta\left(\mathbf{C}_{\Delta\mathbf{m}}^{-1} + \mathbf{D}^T\mathbf{A}\mathbf{D}\right)\boldsymbol{\mu}\right) \end{aligned} \tag{15}$$

where $\mathbf{A}\left(\Delta\mathbf{m}\right) = \dfrac{1}{\sqrt{k_l^4 + k_l^2\left[\mathbf{D}\left(\Delta\mathbf{m} - \boldsymbol{\mu}\right)\right]_l^T\left[\mathbf{D}\left(\Delta\mathbf{m} - \boldsymbol{\mu}\right)\right]_l}}$.

As shown in the solution formula (15), the element A on the right side of the solution formula also contains $\Delta\mathbf{m}$, so iterative reweighed least-squares (IRLS) algorithm is adopted to solve this solution formula. In addition, $\mathbf{L} = \dfrac{\partial\mathbf{G}\left(\mathbf{m}_1\right)}{\partial\mathbf{m}}$ is value of the first order partial derivative matrix at the elastic parameter $\mathbf{m}_1$. Therefore, it is necessary to perform pre-stack inversion based on the exact Zoeppritz equations on the matched baseline survey data to obtain the forward operator matrix L. This can be obtained by using the nonlinear AVO inversion method based on the exact Zoeppritz equations proposed by Zhou et al (2017).

Examples of Application

Model Test

In this part, the single-well model is used to test the feasibility and stability of the new method. Fig. 1 shows the comparison of pre-development and post-development logging curves. The red line is the pre-development logging curve (before fluid replacement), and the blue line is the post-development logging curve (after fluid replacement in the actual reservoir area by using Gassmann equation). The solid line in Fig. 2 shows the real elastic parameter changes obtained by subtracting the logging curves before from curves after development, and the dotted line is the initial model obtained by smoothing the real changes multiple times. Based on the logging data shown in Fig. 1, the synthetic pre-stack angle gathers are synthesized using the exact Zoeppritz equations. These synthetic data sets consist of ten traces with angle range of 4° to 40° and shown in Fig. 3. In the forward modeling process, the main frequency is 30Hz and the sampling interval is 2ms.

Fig. 4(a) shows the results of the independent time-lapse seismic inversion by using the exact Zoeppritz equations based inversion method. From the inversion results, we can see that the independent inversion easil gives a false result in the non-injection-producing area. Fig. 4(b) shows the time-lapse seismic difference inversion results by using inversion method based on the exact Zoeppritz equations with Cauchy prior distribution. From the comparison of Fig. 4(a) and 4(b), the results of difference inversion are significantly improved, especially for S- wave velocity and density. Fig. 4(c) shows the inversion results of the changes in three elastic parameters obtained using the proposed method. From the comparison of Fig. 4(b) and 4(c), the proposed method can capture the true parameter value significantly better by effectively suppressing side lobes. In order to further demonstrate the advantages of the new method, the results of time-lapse seismic inversion based on approximation formula are presented. Fig. 4(d) shows the inversion results of elastic parameters changes obtained using the method of time-lapse seismic difference inversion based on Aki-Richards approximation formula. By comparing Fig s. 4(c)-(d), the accuracy of the proposed method is obviously higher than that of the conventional method.

In addition, random noises with signal-to-noise ratio (root-mean-square amplitude ratio) of 4, 2 and 1 are added to the baseline and monitor survey data respectively, and then subtracted to obtain the corresponding noisy difference data. These data are shown in Fig. 5 and used to test the anti-noise performance of the proposed inversion method. The inversion results of different noisy data are shown in Fig. 6 with the S/N of 4, 2 and 1, respectively. It can be seen from these inversion results that the proposed method has a good anti-noise property. To sum up, the proposed inversion method can reasonably estimate

the elastic parameters changes from the time-lapse seismic difference data while remaining stable.

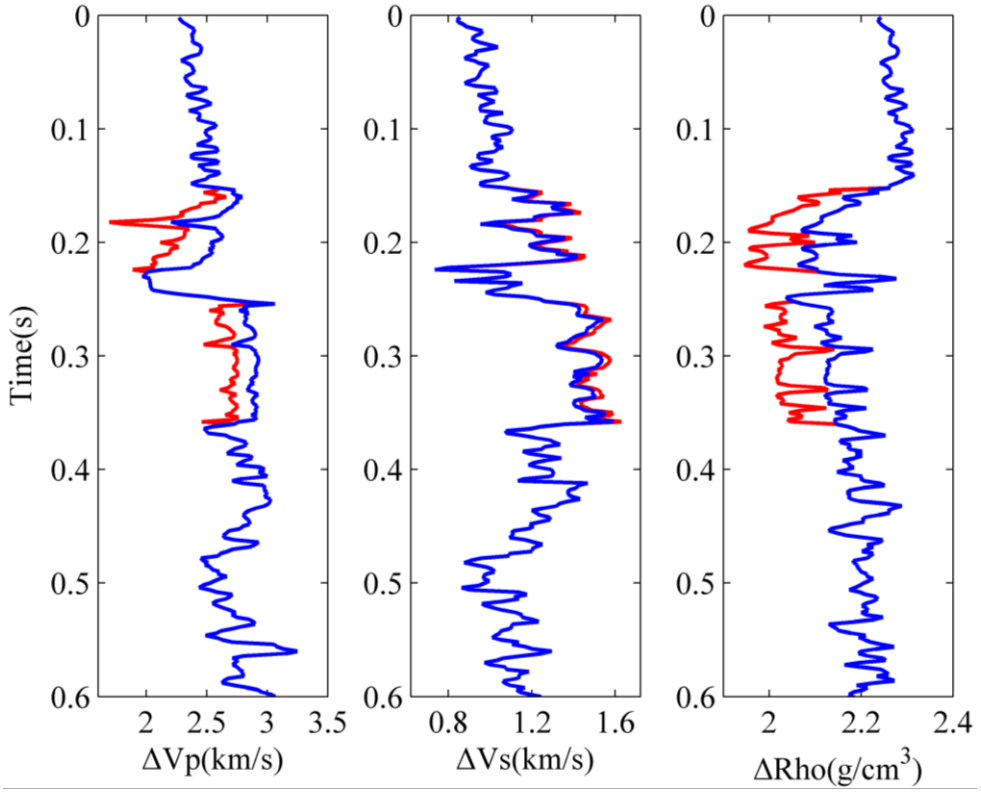

Figure 1. Comparison of pre-development and post-development logging curves. The red line indicates the pre-development logging curve and the blue line indicates the post-development logging curve.

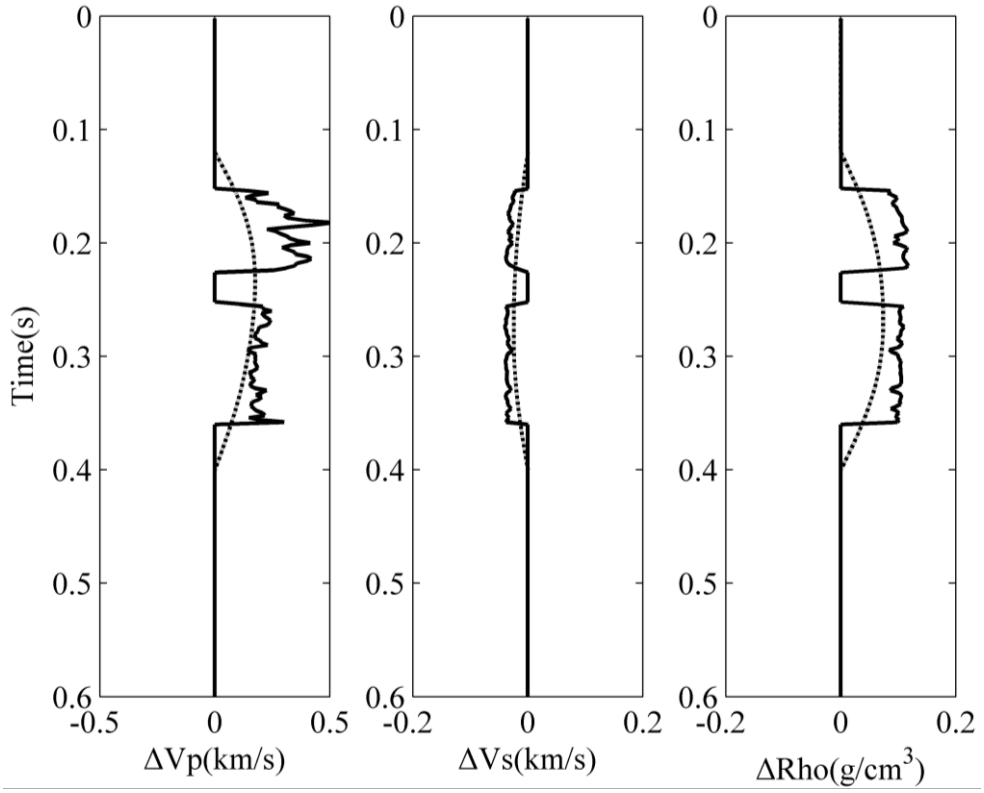

Figure 2. True model data (solid line) and initial model data (dashed line) of elastic parameter changes.

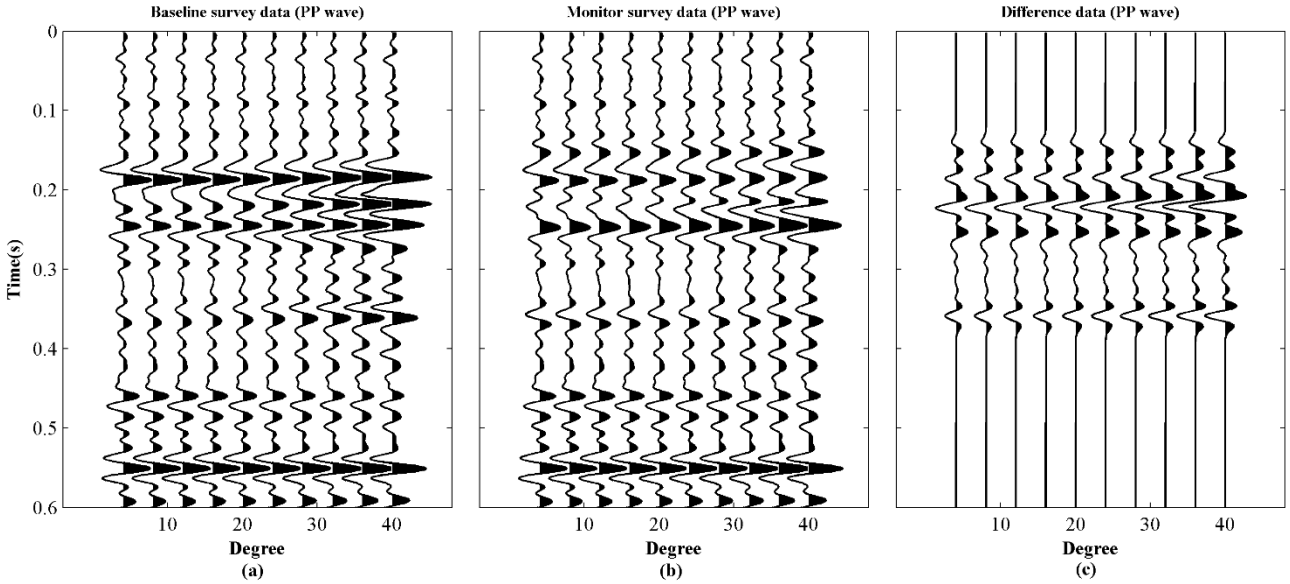

Figure 3. Synthetic PP wave pre-stack angle gathers. (a) Baseline survey data, (b) monitor survey data and (c) difference data.

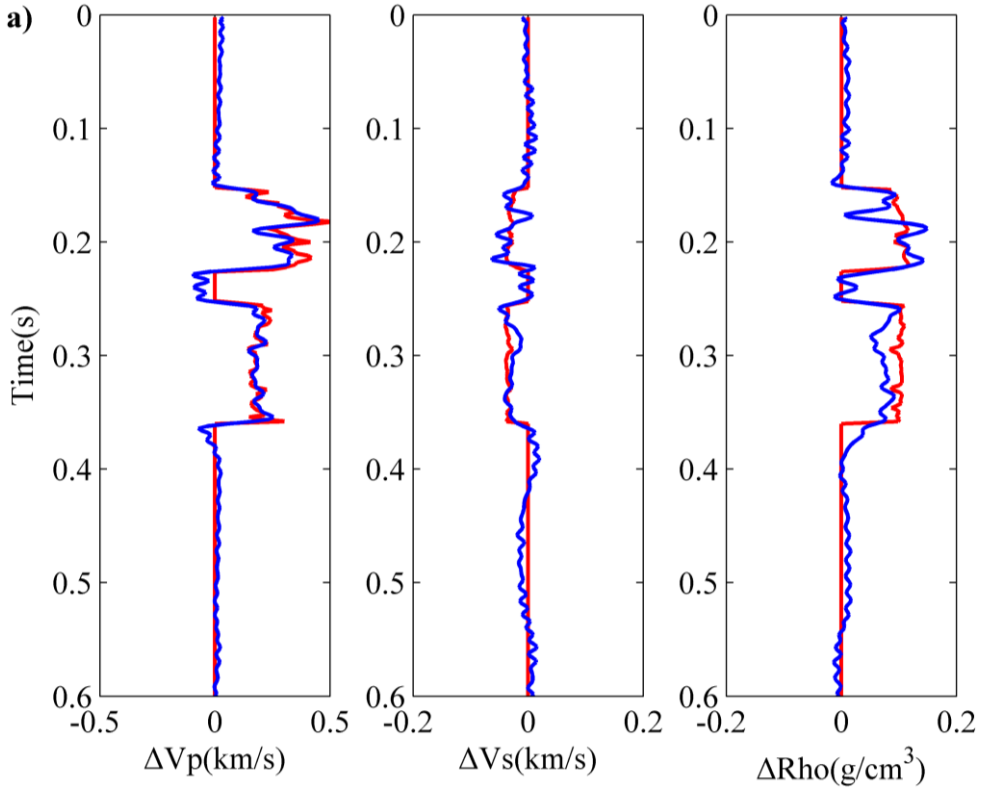

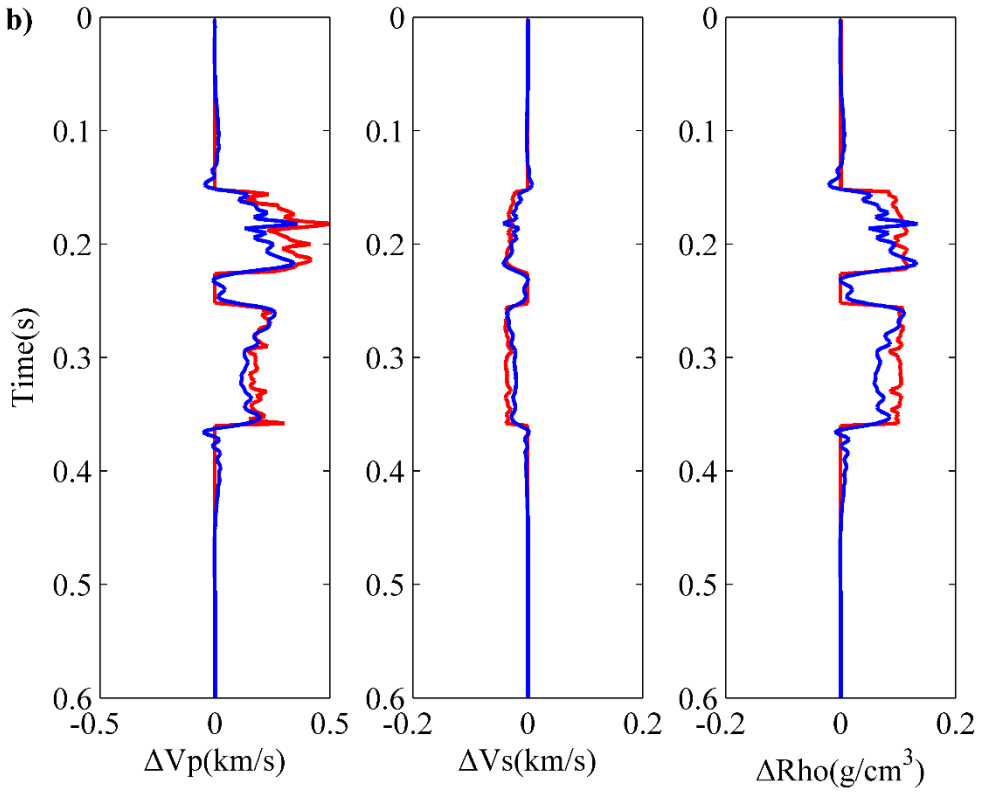
b)
Time(s)
0
0.1
0.2
0.3
0.4
0.5
0.6
-0.5
0
0.5
ΔVp(km/s)
-0.2
0
0.2
ΔVs(km/s)
ΔRho(g/cm3)

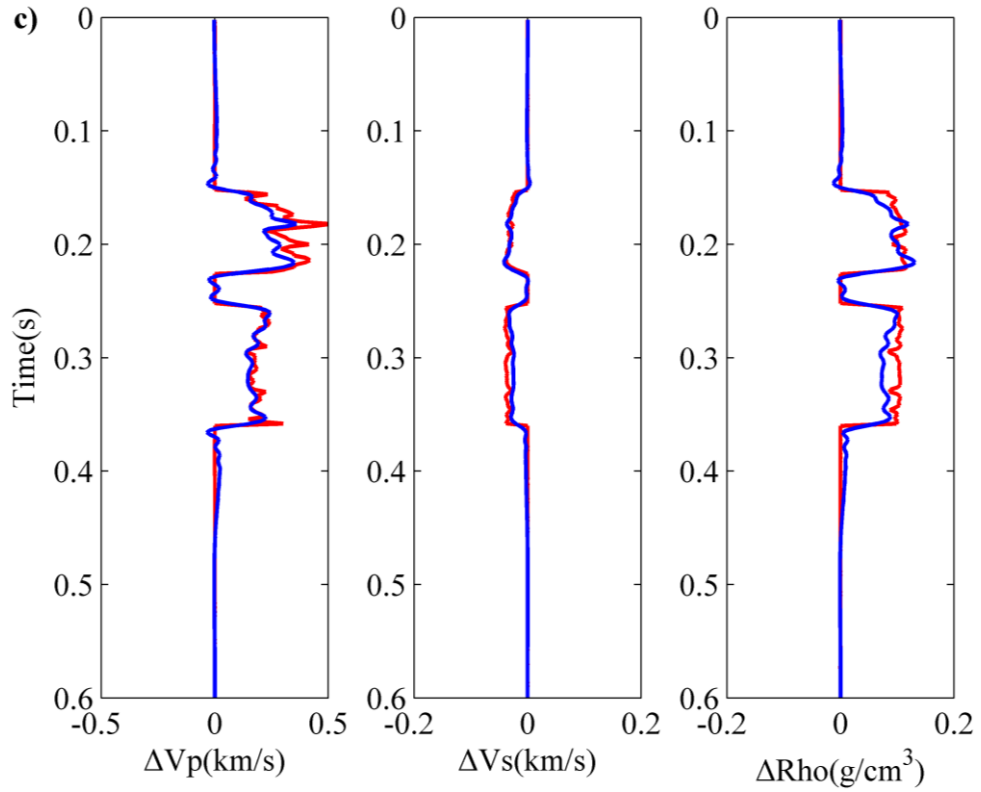
c)
Time(s)
0
0.1
0.2
0.3
0.4
0.5
0.6
-0.5
0
0.5
ΔVp(km/s)
-0.2
0
0.2
ΔVs(km/s)
ΔRho(g/cm3)

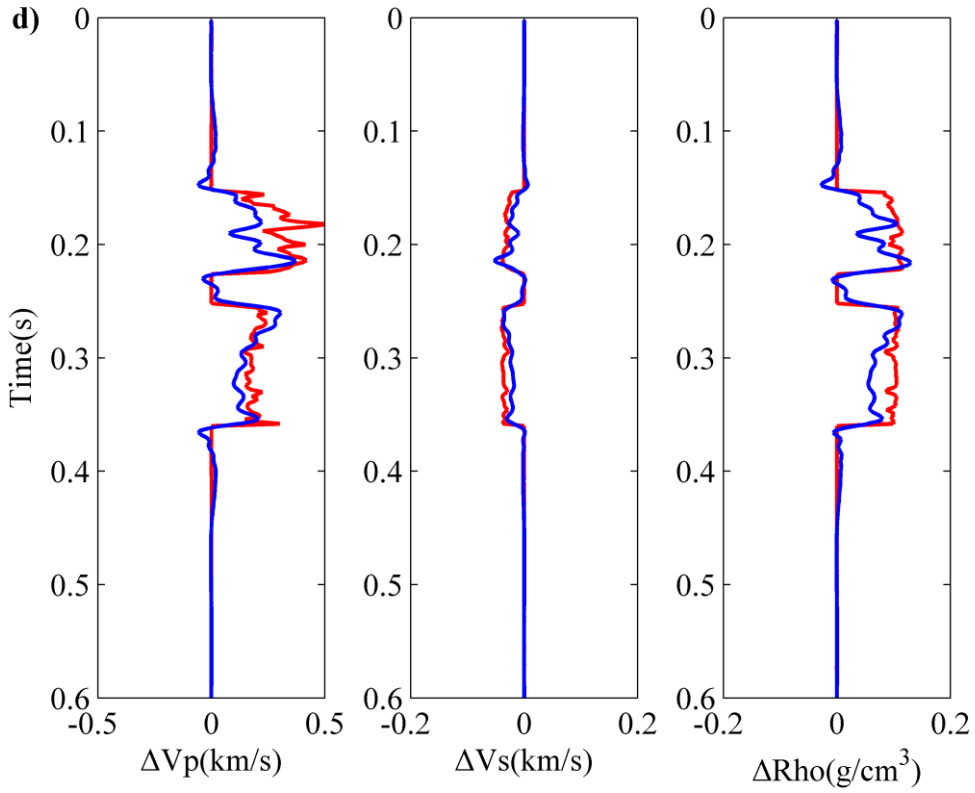

Figure 4. Inversion results. The blue line indicates the inversion result and the red line indicates the true model data. (a) The independent inversion results based on the exact Zoeppritz equations, (b) The difference inversion results based on the exact Zoeppritz equations with Cauchy prior distribution, (c) the inversion results of the proposed method and (d) the difference inversion results based on Aki-Richards approximation formula.

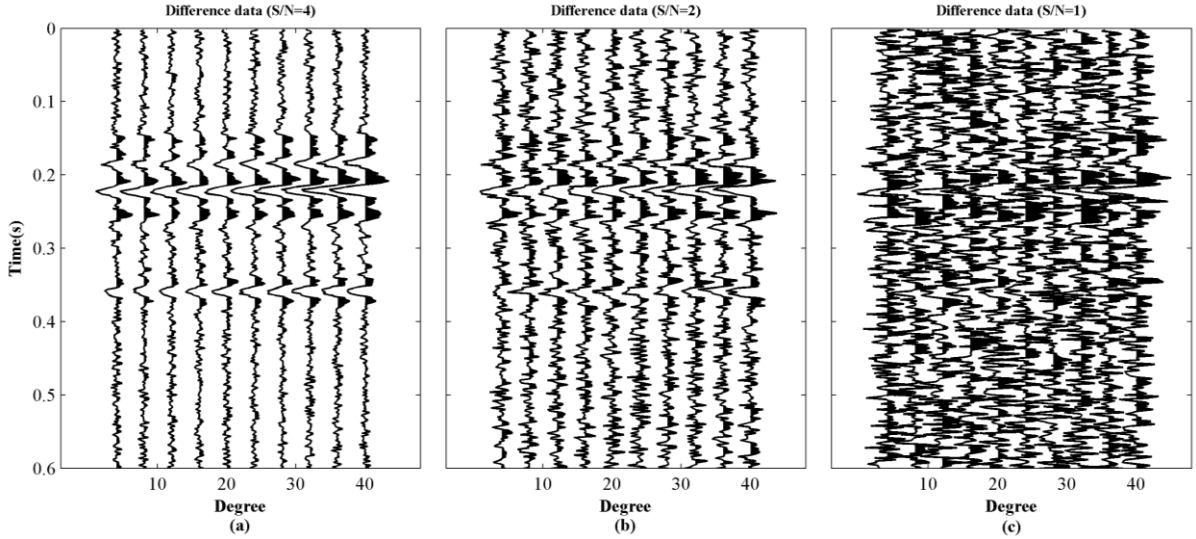

Figure 5. Synthetic difference data with added random noise. (a) S/N=4, (b) S/N=2 and (c) S/N=1.

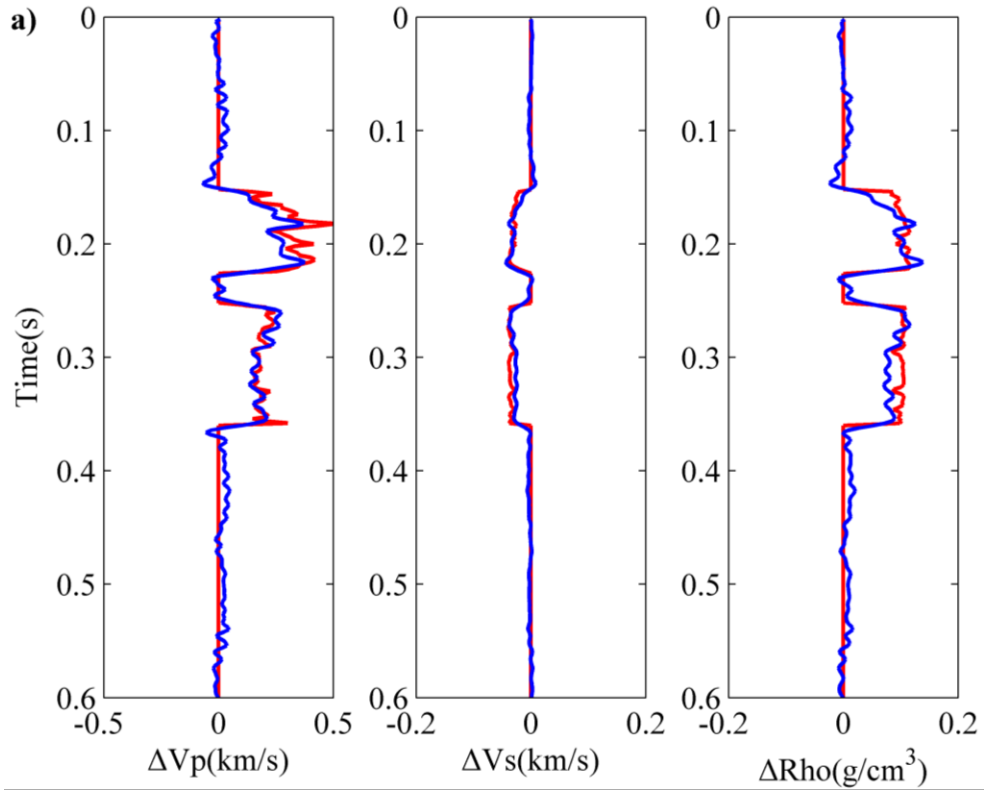
a)
Time(s)
0
0.1
0.2
0.3
0.4
0.5
0.6
-0.5
0
0.5
ΔVp(km/s)
-0.2
0
0.2
ΔVs(km/s)
ΔRho(g/cm3)

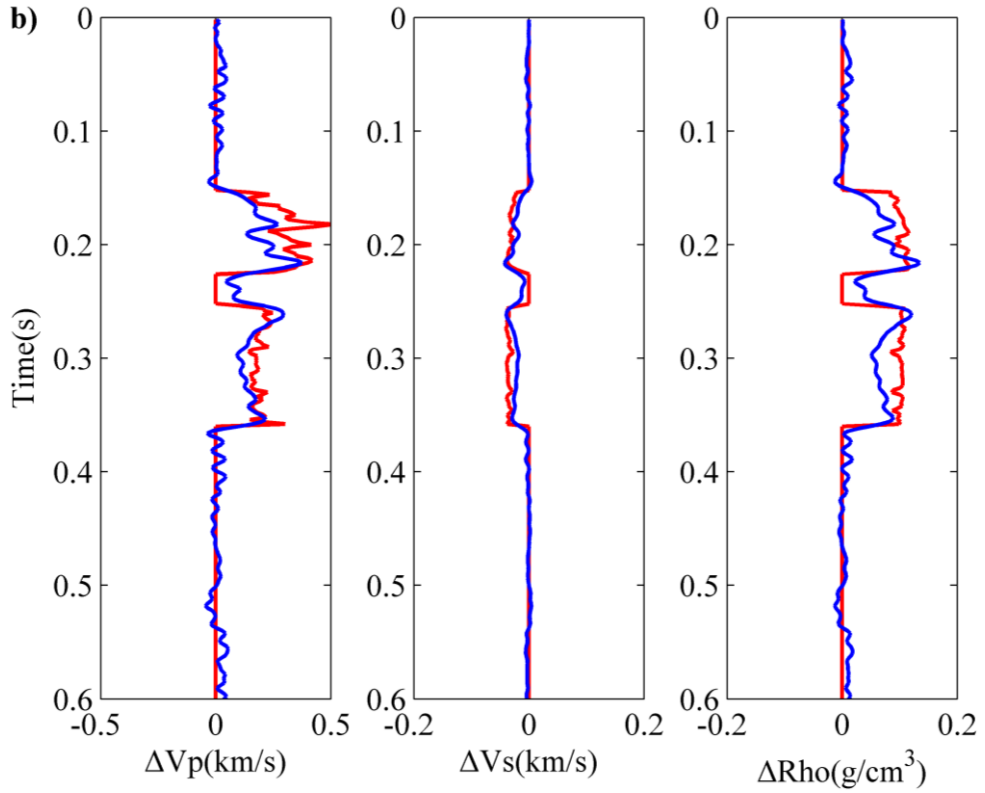
b)
Time(s)
0
0.1
0.2
0.3
0.4
0.5
0.6
-0.5
0
0.5
ΔVp(km/s)
-0.2
0
0.2
ΔVs(km/s)
ΔRho(g/cm3)

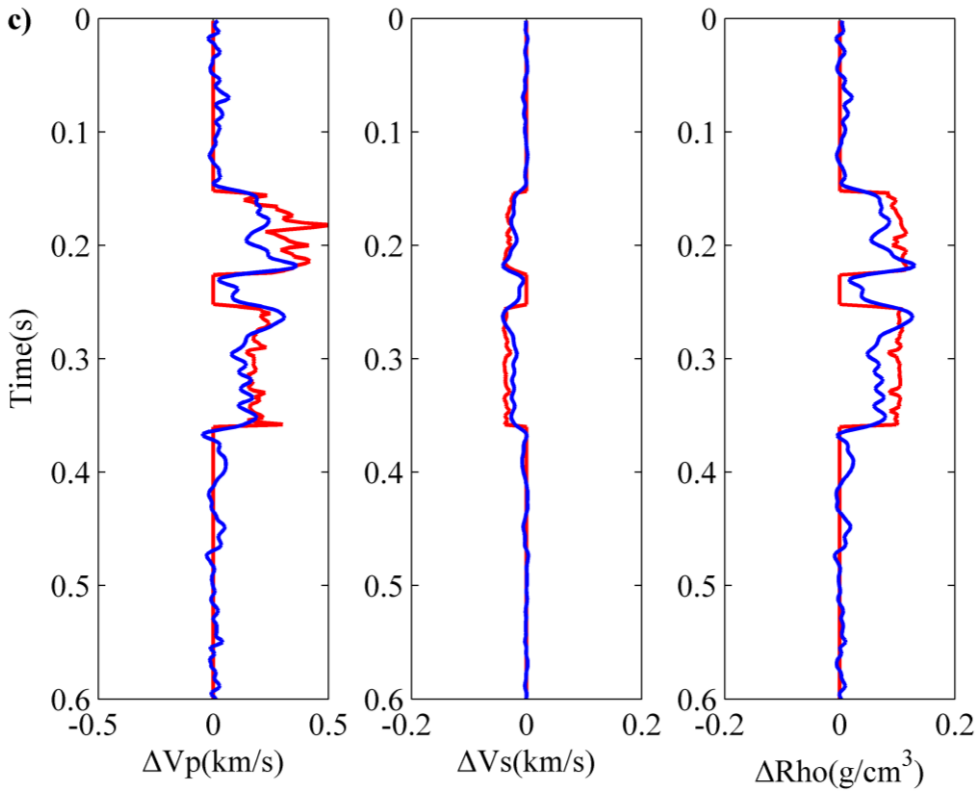

Figure 6. Inversion results of noisy data. (a) S/N=4, (b) S/N=2 and (c) S/N=1.

Field Data Application

Field data were obtained from a survey line of an offshore gas field in China. The structure of this field is a large simple short-axis anticline formed by the local uplift deformation of the overlying strata that is caused by deep mudstone with overarching conditions of high temperature and pressure, which has the characteristics of large trap area, large closure and shallow burial. The base data and monitor data of this survey line contain the angle gathers data corresponding to three angles of 10^o, 20^o and 30^o, respectively. Fig. 7 shows the difference data section when the incidence angle is 20^o, and the red rectangle in the figure is a gas-bearing region.

Firstly, the forward operator matrix L is obtained by using the baseline survey data to perform the inversion based on the exact Zoeppritz equations. Then, this matrix is applied to time-lapse seismic difference inversion, and the field data inversion results (Figure 8) for P-wave velocity changes (8(a)) S-wave velocity changes (8(b)) and density changes (8(c)) estimated by using the proposed method . As can be seen from the figure, the injection-production area shows obvious changes in elastic parameters, and the overburden also changes in elastic parameters due to pressure changes caused by oil and gas exploitation, while the false identification of changes in elastic parameters changes in other non-injection-production

areas is effectively suppressed. The Synthetic section of the inversion results (incidence angle is 20^{o}) is shown in Fig. 9. Comparing Figs. 7 and 9, the synthetic seismic data of the inversion results matched well with the input difference data. Fig. 10 shows the enlarged drawing of the field data inversion results shown in Fig. 8. It can be seen that the inversion results of the proposed method are in good agreement with the production Well A. From the above analysis, the inversion results in this study are consistent with the real field situation, indicating that the proposed method can effectively suppress the false identification, highlight the changes of reservoir parameters, and better reflect the actual changes of reservoir oil and gas. In addition, we can also see from Fig. 8 that the inversion results obtained by the proposed method have higher resolution and can provide high-resolution seismic information for the detailed description of reservoir, which is of great significance for the application of time-lapse seismic inversion in the working area.

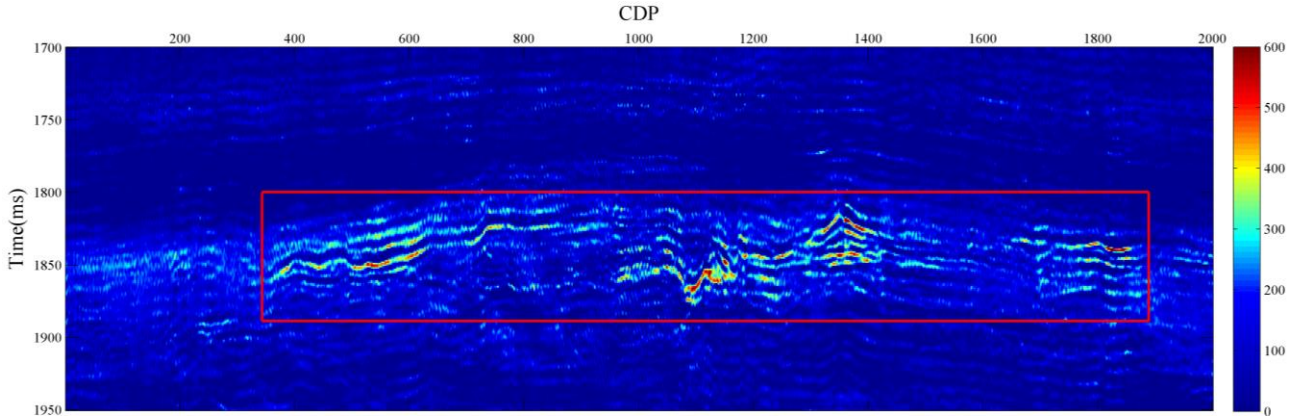

Figure 7. Difference data section when the incidence angle is 20^{o}.

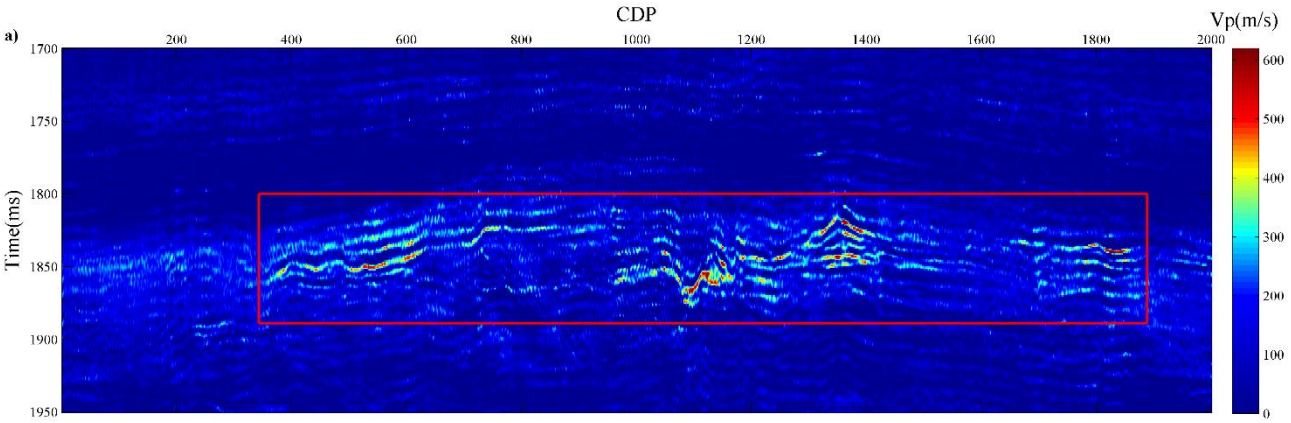

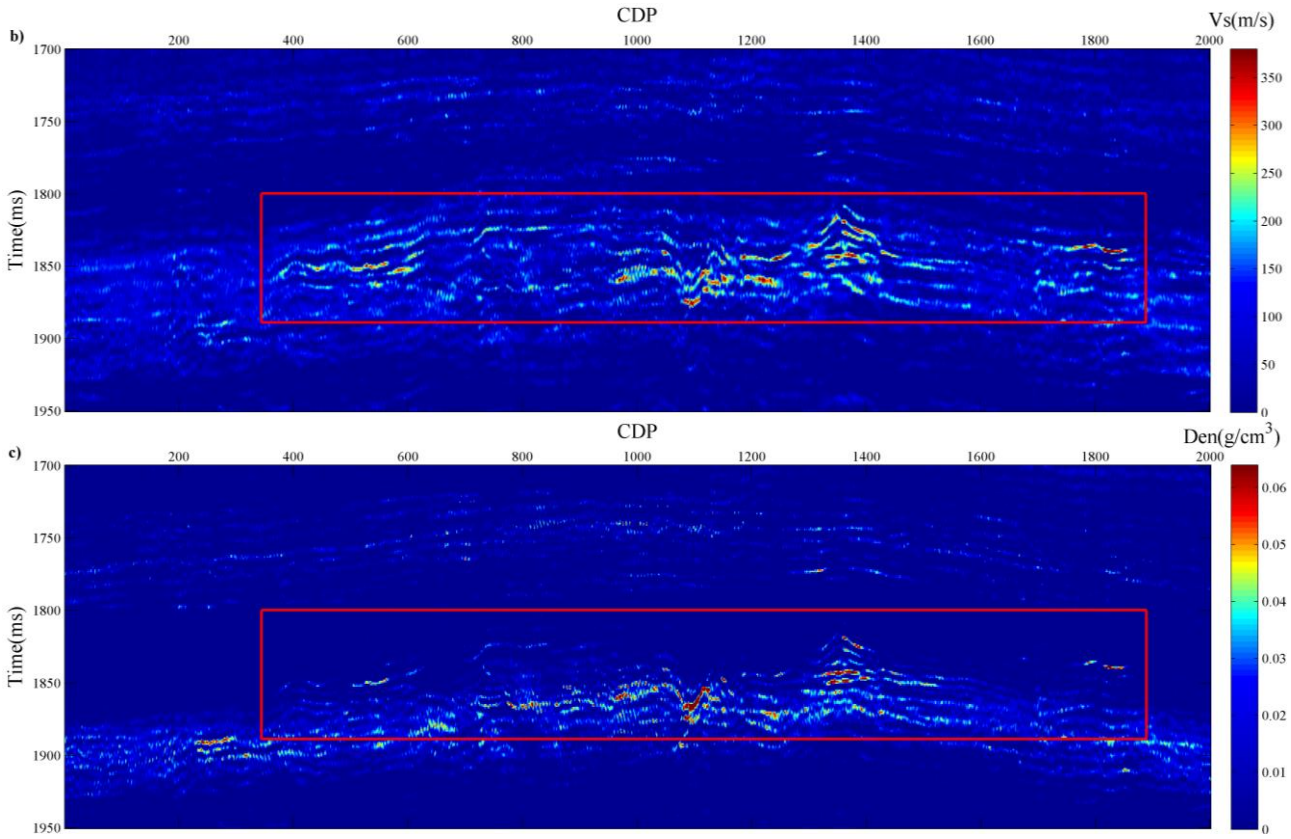

Figure 8. Field data inversion results. (a) P-wave velocity changes, (b)S-wave velocity changes and (c)density changes.

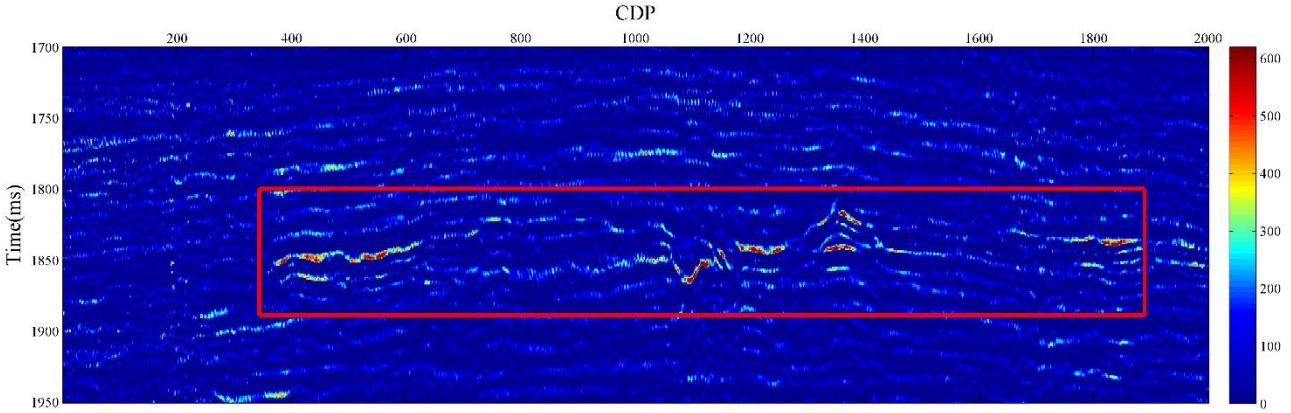

Figure 9. Synthetic section of the inversion results (incidence angle is 20^{o}).

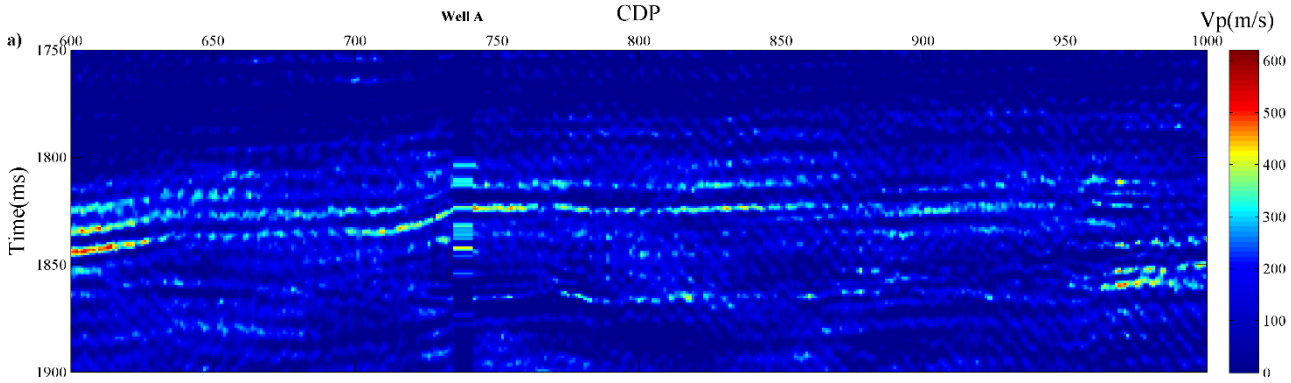

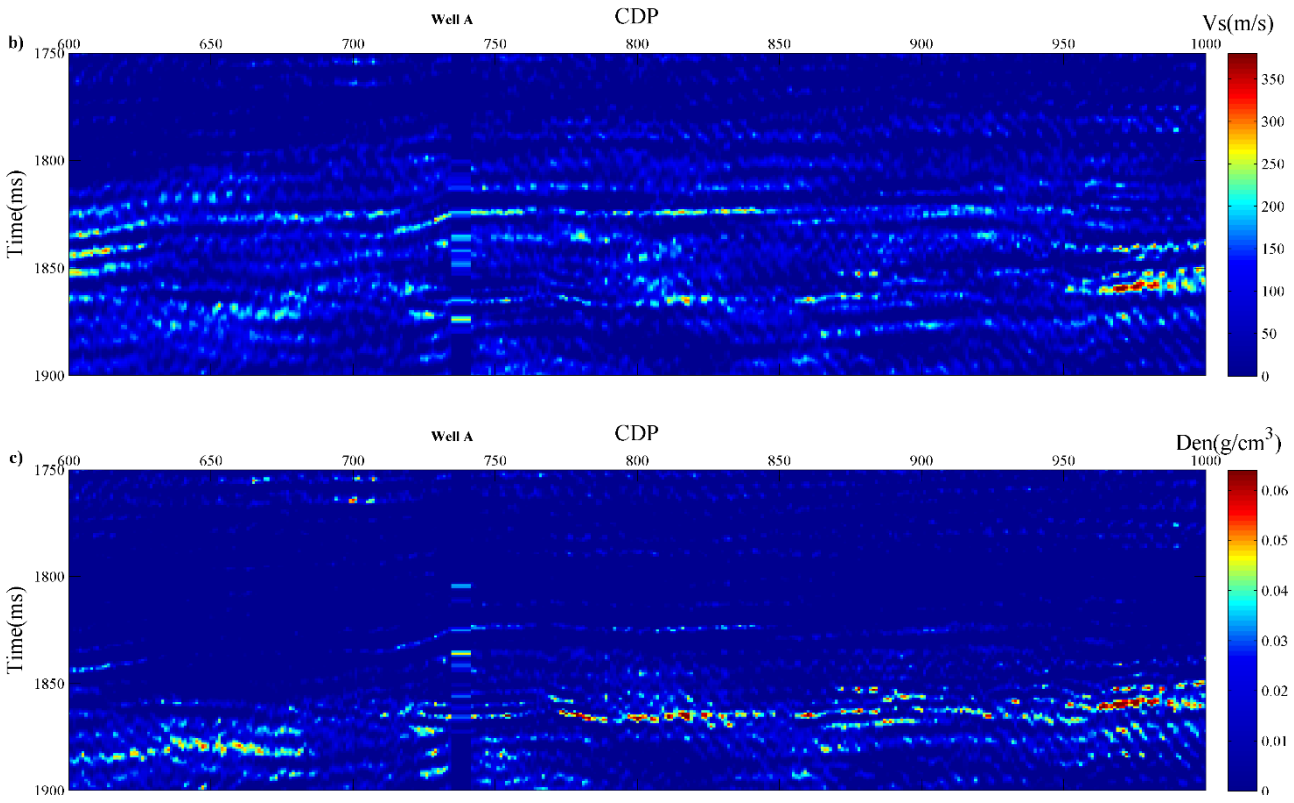

Figure 10. The enlarged drawing of the field data inversion results. (a) P-wave velocity changes, (b) S-wave velocity changes and (c) density changes.

Conclusion

We have derived the forward equation of time-lapse seismic difference data based on the exact Zoeppritz equations and then used it to construct the time-lapse seismic AVA difference inversion objective function. This can effectively reduce the error caused by the poor calculation accuracy of the approximate formula. Meanwhile, because the of time-lapse seismic inversion parameters distribution is discontinuous, a priori model containing the differentiable Laplace blockiness constraint term is introduced to enhance the accuracy of inversion results. Test of application to real data show that the proposed method can accurately estimate the P- and S-wave velocities and density changes caused by the production of hydrocarbons. This is of great significance in the detailed description of reservoirs in the middle and late stage of development and in the identification of favorable well locations. Compared with the inversion results based on synthetic data, the inversion results of the proposed method are obviously superior to those based on the approximate formulas, which verifies the feasibility and superiority of this method. From the inversion results of noisy data, we can see that the proposed method has good anti-noise property.

The proposed method is an inversion method based on well-constraints, which needs to obtain statistically the covariance matrix and scale factor from the logging data. The quality of this prior information directly affects the accuracy of inversion results. In addition, matching quality of baseline survey and monitor data will also seriously affect the accuracy of inversion results.

Acknowledgments

This work was financially supported by the National Natural Science Foundation of China (41904116, 41874156, 41774129 and 41774131), Doctoral fund of Hunan University of Science and Technology (E518B2) and Key State Science and Technology Project (2016ZX05033-003-008, 2016ZX05024001-004).

References

Abubakar, A., Berg, P.M., and Fokkema, J.T., 2001, A feasibility study on nonlinear inversion of time-lapse seismic data: in Expanded Abstracts: 71th Annual International Meeting, Society of Exploration Geophysics, 1664–1667.

Ayeni, G., Tang, Y., and Biondi, B., 2009, Joint preconditioned least-squares inversion of simultaneous source time-lapse seismic data sets: 79th Annual International Meeting, Society of Exploration Geophysics, 3914–3918.

Buland, A., and Ouair, Y.E., 2006, Bayesian time-lapse inversion: Geophysics, **71**, R43–R48.

Chen, Y., Han, B., Xiao, L., and Chen, X.H., 2010, Multiscale total variation method and its application on time-lapse seismic: Chinese J. Geophys. (in Chinese), **53(8)**, 1883–1892.

Eidsvik, J., and Theune, U., 2009, Blocky inversion of time-lapse seismic AVO data: 79th Annual International Meeting, Society of Exploration Geophysics, 3820–3824.

Gluck, S., Deschizeaux, B., Mignot, A., Pinson, C., and Huguet, F., 2000, Time-lapse impedance inversion of post-stack seismic data: 70th Annual International Meeting, Society of Exploration Geophysics, 1509–1512.

Grana, D., and Mukerji, T., 2015, Bayesian inversion of time-lapse seismic data for the estimation of static reservoir properties and dynamic property changes: Geophysical Prospecting, **63**, 637–655.

Hicks, E., Hoeber, H., Houbiers, M., Lescoffit, S.P., Ratcliffe, A., and Vinje, V., 2016, Time-lapse full-waveform inversion as a reservoir-monitoring tool — A North Sea case study: The Leading Edge, **35**, 850–858.

Kato, A., and Stewart, R.R., 2010, Joint AVO inversion for time-lapse elastic reservoir properties: Hangingstone heavy oilfield, Alberta: 80th Annual International Meeting, Society of Exploration Geophysics, 4432–4437.

Kamei, R., Jang, U.G., Lumley, D., Mouri, T., Nakatsukasa, M., Kato, A., and Takanashi, M., 2017, Time-lapse full waveform inversion for monitoring nearsurface microbubble injection: 79th Annual International Meeting, European Association of Geoscientists & Engineers.

Kamei, R., and Lumley, D., 2017, Full waveform inversion of repeating seismic events to estimate time-lapse velocity changes: Geophysical Journal International, **209**, 1239–1264.

Landr, M., 2001, Discrimination between pressure and fluid saturation changes from time-lapse seismic data: Geophysics, **66(3)**, 836–844.

Li, J.Y., Chen, X.H., Hao, Z.J., and Rui, Z.H., 2005, A study on multiple time-lapse seismic AVO inversion: Chinese J. Geophys. (in Chinese), **48(4)**, 902–908.

Li, J.Y., Wang, S.D., and Chen, X.H., 2011, Time-lapse seismic elastic impedance difference inversion and application: 81th Annual International Meeting, Society of Exploration Geophysics, 2494-2496.

Liu, X.Y., Chen, X.H., Li, J.Y., Zhou, L., and Guo, K.K., 2016, Reservoir physical property prediction based on kernel-Bayes discriminant method: Acta Petrolei Sinica, **37(7)**, 878–886.

Liu, X.Y., Li, J.Y., Chen, X.H., Guo, K.K., Li, C., Zhou, L., and Cheng, J.W., 2018, Stochastic inversion of facies and reservoir properties based on multi-point geostatistics: Journal of Geophysics and Engineering, **15(6)**, 2455–2468.

Lu, J., Yang, Z., Wang, Y., and Shi, Y., 2015, Joint PP and PS AVA seismic inversion using exact Zoeppritz equations: Geophysics, **80(5)**, R239–R250.

Raknes, E.B., Arntsen, B., 2015, A numerical study of 3D elastic time-Tlapse full-waveform inversion using multicomponent seismic data: Geophysics, **80(6)**, R303–R315.

Stewart, R.R., 1990, Joint P and P-SV inversion: CREWES Research Report 2, 112–115.

Sarkar, S., Gouveia, W.P., and Johnston, D.H., 2003, On the inversion of time-lapse seismic data, 73th Annual International Meeting, Society of Exploration Geophysics, 1489–1492.

Todoeschuck, J.P., Jensen, O.G., and Labonte, S., 1990, Gaussian scaling noise model of seismic reflection sequences: Evidence from well logs: Geophysics, **55(4)**, 480–484.

Tura, A., and Lumley, D.E., 1999, Estimating pressure and saturation changes from time-lapse AVO data, 69th Annual International Meeting, Society of Exploration Geophysics, 1655–1658.

Theune, U., Jensas, I.Ø., and Eidsvik, J., 2010, Analysis of prior models for a blocky inversion of seismic AVA data: Geophysics, **75(3)**, C25–C35.

Tang, W., Li, J.Y., Zhou, L., and Zhang, J., 2018, Time-lapse impedance difference inversion of poststack seismic data, 88th Annual International Meeting, Society of Exploration Geophysics, 5343–5347.

Wang, S.D., and Wang, B., 2012, Time-lapse Bayesian AVO waveform inversion: Chinese J. Geophys. (in Chinese), **55(7)**, 2422–2431.

Zhang, F.Q., Wei, F.J., Wang, Y.C., Wang, W.J., and Li, Y., 2013, Generalized linear AVO inversion with the priori constraint of trivariate Cauchy distribution based on Zoeppritz equation: Chinese J. Geophys. (in Chinese), 56(6), 2098–2115.

Zhi, L., Gu, H., and Li, Y., 2016, The time-lapse AVO difference inversion for changes in reservoir parameters: Journal of Geophysics and Engineering, **13**, 899–911.

Zhi, L.X., Chen, S.Q., and Li, X.Y., 2016, Amplitude variation with angle inversion using the exact Zoeppritz equations — Theory and methodology: Geophysics, **81(2)**, N1–N15.

Zhou, L., Li, J.Y., and Chen, X.H., 2016, Nonlinear three term AVO inversion based on exact Zoeppritz equation: Chinese J. Geophys. (in Chinese), **59(7)**, 2663–2673.

Zhou, L., Li, J.Y., Chen, X.H., Liu, X.Y., and Chen, L., 2017, Pre-stack AVA inversion of exact Zoeppritz equations based on modified Trivariate Cauchy distribution: Journal of Applied Geophysics, **138**, 80–90.

Zhi, L., and Gu, H., 2018, Time-lapse joint AVO inversion using generalized linear method based on exact Zoeppritz equations: Journal of Applied Geophysics, **150**, 195–207.

Appendix A

THE DERIVATION OF THE FIRST ORDER PARTIAL DERIVATIVE MATRIX

The first order partial derivative of $\mathbf{G}(\mathbf{m})$ can be written as:

$$\frac{\partial \mathbf{G}(\mathbf{m})}{\partial \mathbf{m}} = \frac{\partial\left(\mathbf{W} \bullet \mathbf{r}(\mathbf{m})\right)}{\partial \mathbf{m}} = \mathbf{W} \bullet \frac{\partial \mathbf{r}(\mathbf{m})}{\partial \mathbf{m}}, \tag{A1}$$

where $\mathbf{W}$ is the wavelet matrix, and $\mathbf{r}(\mathbf{m})$ represents the reflection coefficients sequence. For a certain angle θ_i, the following expression can be given:

$$\frac{\partial \mathbf{G}_{(\theta_i)}}{\partial \mathbf{m}} = \mathbf{W} \bullet \frac{\partial \mathbf{r}_{(\theta_i)}}{\partial \mathbf{m}} = \mathbf{W} \bullet \begin{bmatrix} \frac{\partial r_{(\theta_i,1)}}{\partial V_{P1}} & \frac{\partial r_{(\theta_i,1)}}{\partial V_{P2}} & 0 & \cdots & \cdots & \frac{\partial r_{(\theta_i,1)}}{\partial V_{S1}} & \frac{\partial r_{(\theta_i,1)}}{\partial V_{S2}} & 0 & \cdots & \cdots & \frac{\partial r_{(\theta_i,1)}}{\partial \rho_1} & \frac{\partial r_{(\theta_i,1)}}{\partial \rho_2} & 0 & \cdots & \cdots \\ 0 & \frac{\partial r_{(\theta_i,2)}}{\partial V_{P2}} & \frac{\partial r_{(\theta_i,2)}}{\partial V_{P3}} & 0 & \cdots & 0 & \frac{\partial r_{(\theta_i,2)}}{\partial V_{S2}} & \frac{\partial r_{(\theta_i,2)}}{\partial V_{S3}} & 0 & \cdots & 0 & \frac{\partial r_{(\theta_i,2)}}{\partial \rho_2} & \frac{\partial r_{(\theta_i,2)}}{\partial \rho_3} & 0 & \cdots \\ \cdots & \cdots & \cdots & \cdots & \cdots & \cdots & \cdots & \cdots & \cdots & \cdots & \cdots & \cdots & \cdots & \cdots & \cdots \\ \cdots & \cdots & 0 & \frac{\partial r_{(\theta_i,N-1)}}{\partial V_{P(N-1)}} & \frac{\partial r_{(\theta_i,N-1)}}{\partial V_{PN}} & \cdots & \cdots & 0 & \frac{\partial r_{(\theta_i,N-1)}}{\partial V_{S(N-1)}} & \frac{\partial r_{(\theta_i,N-1)}}{\partial V_{SN}} & \cdots & \cdots & 0 & \frac{\partial r_{(\theta_i,N-1)}}{\partial \rho_{N-1}} & \frac{\partial r_{(\theta_i,N-1)}}{\partial \rho_N} \\ \cdots & \cdots & \cdots & 0 & \frac{\partial r_{(\theta_i,N)}}{\partial V_{PN}} & \cdots & \cdots & \cdots & 0 & \frac{\partial r_{(\theta_i,N)}}{\partial V_{SN}} & \cdots & \cdots & \cdots & 0 & \frac{\partial r_{(\theta_i,N)}}{\partial \rho_N} \end{bmatrix}_{(N\times 3N)}. \tag{A2}$$

Extending equation (A2) to the nth input angles situation, the first order partial derivative matrix will become a $(n\times N)\times 3N$ matrix. Extending to the situation of joint PP-PS wave inversion, $\frac{\partial \mathbf{G}(\mathbf{m})}{\partial \mathbf{m}}$ will becomes a $(2n\times N)\times 3N$ matrix eventually.

The exact Zoeppritz equations are expressed as follows:

$$\begin{bmatrix} -\sin\theta_1 & -\cos\varphi_1 & \sin\theta_2 & \cos\varphi_2 \\ \cos\theta_1 & -\sin\varphi_1 & \cos\theta_2 & -\sin\varphi_2 \\ \sin 2\theta_1 & \dfrac{V_{P1}}{V_{S1}}\cos 2\varphi_1 & \dfrac{\rho_2 V^2_{S2} V_{P1}}{\rho_1 V^2_{S1} V_{P2}}\sin 2\theta_2 & \dfrac{\rho_2 V_{S2} V_{P1}}{\rho_1 V^2_{S1}}\cos 2\varphi_2 \\ -\cos 2\varphi_1 & \dfrac{V_{S1}}{V_{P1}}\sin 2\varphi_1 & \dfrac{\rho_2 V_{P2}}{\rho_1 V_{P1}}\cos 2\varphi_2 & -\dfrac{\rho_2 V_{S2}}{\rho_1 V_{P1}}\sin 2\varphi_2 \end{bmatrix} \begin{bmatrix} r_{PP} \\ r_{PS} \\ t_{PP} \\ t_{PS} \end{bmatrix} = \begin{bmatrix} \sin\theta_1 \\ \cos\theta_1 \\ \sin 2\theta_1 \\ \cos 2\varphi_1 \end{bmatrix}, \tag{A3}$$

Then, the above equation can be expressed by matrix form:

$$\mathbf{AR} = \mathbf{b}, \tag{A4}$$

So, we can obtain: $\mathbf{A}=\begin{bmatrix} -\sin\theta_1 & -\cos\varphi_1 & \sin\theta_2 & \cos\varphi_2 \\ \cos\theta_1 & -\sin\varphi_1 & \cos\theta_2 & -\sin\varphi_2 \\ \sin 2\theta_1 & \dfrac{V_{P1}}{V_{S1}}\cos 2\varphi_1 & \dfrac{\rho_2 V^2_{S2} V_{P1}}{\rho_1 V^2_{S1} V_{P2}}\sin 2\theta_2 & \dfrac{\rho_2 V_{S2} V_{P1}}{\rho_1 V^2_{S1}}\cos 2\varphi_2 \\ -\cos 2\varphi_1 & \dfrac{V_{S1}}{V_{P1}}\sin 2\varphi_1 & \dfrac{\rho_2 V_{P2}}{\rho_1 V_{P1}}\cos 2\varphi_2 & -\dfrac{\rho_2 V_{S2}}{\rho_1 V_{P1}}\sin 2\varphi_2 \end{bmatrix}$, $\mathbf{R}=\begin{bmatrix} r_{PP} \\ r_{PS} \\ t_{PP} \\ t_{PS} \end{bmatrix}$ and $\mathbf{b}=\begin{bmatrix} \sin\theta_1 \\ \cos\theta_1 \\ \sin 2\theta_1 \\ \cos 2\varphi_1 \end{bmatrix}$.

The derivative of both sides of equation (A4) with respect to P- and S- wave velocities and density can be written as:

$$\frac{\partial \mathbf{A}}{\partial m^i}\mathbf{R} + \mathbf{A}\frac{\partial \mathbf{R}}{\partial m^i} = \frac{\partial \mathbf{b}}{\partial m^i}, \qquad i = 1,2,3,4,5,6, \tag{A5}$$

Then, the first order partial derivative of the reflection and transmission coefficient with respect to P- and S- wave velocities and density can be given:

$$\frac{\partial \mathbf{R}}{\partial m^i} = \mathbf{A}^{-1}\left(-\frac{\partial \mathbf{A}}{\partial m^i}\mathbf{A}^{-1}\mathbf{b} + \frac{\partial \mathbf{b}}{\partial m^i}\right), \qquad i = 1,2,3,4,5,6. \tag{A6}$$

Eventually, by setting $\mathbf{m}=\mathbf{m}_1$ and combining the above derivation, we can obtain the new forward operator $\mathbf{L}$.